1987

The Engineering Society
For Advancing Mobility
Land Sea Air and Space

400 COMMONWEALTH DRIVE WARRENDALE, PA 15096

SAE Technical Paper Series

870164

Early Flame Development and Burning Rates in Spark Ignition Engines and Their Cyclic Variability

James C. Keck and John B. Heywood
Massachusetts Institute of Technology
Cambridge, MA

Georg Noske
University of Karlsruhe
Karlsruhe, West Germany

International Congress and Exposition
Detroit, Michigan
February 23—27, 1987

870164

Early Flame Development and Burning Rates in Spark Ignition Engines and Their Cyclic Variability

James C. Keck and John B. Heywood
Massachusetts Institute of Technology
Cambridge, MA

Georg Noske
University of Karlsruhe
Karlsruhe, West Germany

ABSTRACT

Experiments by Gatowski and Heywood have been analyzed to obtain both qualitative and quantitative information on early flame development and burning rates in a square piston premixed spark-ignition engine. Flame growth was observed using high speed Schlieren photography and simultaneous pressure records were obtained using piezo-electric transducers. To study the effects of in-cylinder gas motion several combinations of shrouded and unshrouded inlet valves, and flat and stepped pistons were used. Spark position was also varied.

The analysis supports the wrinkled laminar flame model of turbulent flame structure in spark-ignition engines. It also suggests that cycle-by-cycle variations in the growth rate and location of the flame kernel at very early times are the major cause of cycle-by-cycle pressure variations in spark-ignition engines.

THE DEVELOPMENT OF SIMPLE AND ACCURATE MODELS of turbulent burning in spark-ignition engines is important for the design and active control of improved automotive engines and is a major objective of current combustion research. To provide the basic information and insight need for such development, a detailed analysis of a unique set of experimental observation by Gatowski and Heywood (1)* of early flame growth and pressure rise in a square cross-section engine has been made. The data consist of high speed Schlieren motion pictures made through the two glass walls of the engine and simultaneous pressure vs. crank angle records. A primary objective of the experiments was to investigate the effects of swirl and squish on flame development, and observations were made for chamber geometries including both unshrouded and shrouded inlet valves, and flat and stepped pistons. The data are a valuable addition to the large body of similar data obtained from engines without significant swirl or squish (2).

The present analysis supports the thin wrinkled multiply-connected laminar flame model for turbulent combustion used by Keck and co-workers (3,4) in their development of the "eddy burning" model of combustion in premixed spark-ignition engines and shows that the model can be used in cases where swirl and squish are present if the base flow is taken into account. It also suggests that cycle-by-cycle variations in the position and growth rate of the flame kernel at very early times are the major cause of cycle-by-cycle fluctuations in the pressure curves for spark-ignition engines.

It should be noted that the basic assumptions of the "eddy burning" model are similar to those of the "laminar flamelet" model developed by Bray,Moss and Libby (5). The mathematical formulation is quite different however.

EXPERIMENTAL APPARATUS AND RESULTS

A schematic diagram of the square piston engine used to obtain the data analyzed in this work is shown in Fig. 1 and extensive descriptions are given in Refs 6 and 7. The important geometrical details of the engine and the fixed operating parameters for the experiments are summarized in Tables 1a and 1b.

The primary variable in the experiments was the combustion chamber geometry and the configurations used are shown in Fig. 2. Four cases were investigated: Base: flat piston with standard inlet valve and spark at location 1; Shroud: flat piston with 180° shrouded inlet valve and spark at location 1; Squish 1: stepped piston with a standard inlet valve and spark at location 1; Squish 2:

* Numbers in parentheses designate references at end of paper.

0148-7191/87/0223-0164$02.50

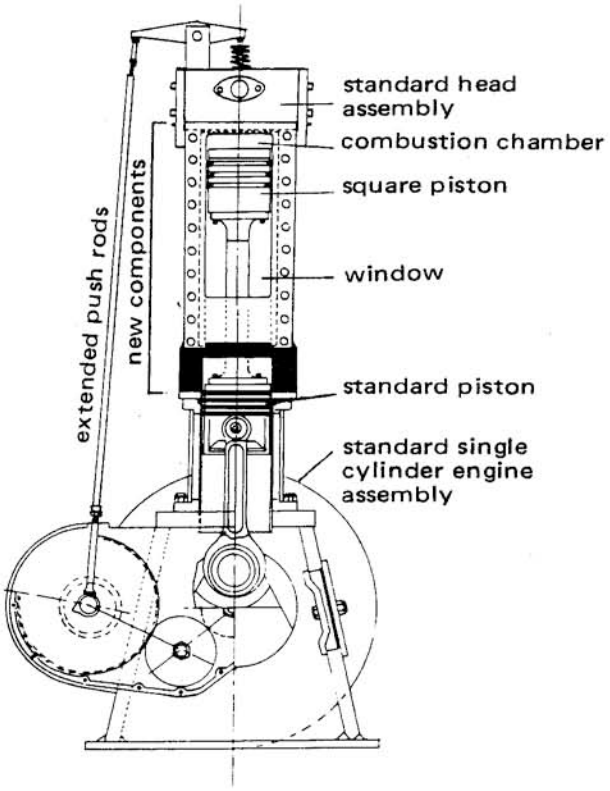

Fig. 1. Schematic of square piston engine.

stepped piston with standard inlet valve and spark at location 2. Spark timing was MBT in all cases and the test conditions at spark are given in Table 2. The symbols used are:

θ	= crank angle
V	= chamber volume
p	= gas pressure
T	= gas temperature
ρ	= gas density
$s_\ell(0)$	= laminar flame speed for 0 residual mass
$s_\ell(0.15)$	= laminar flame speed for 15% residual mass
u_{in}	= mean inlet gas speed
Ma_{in}	= inlet Mach number
u_{AX}	= axial gas velocity
u_{SQ}	= squish velocity
u_{SW}	= swirl velocity

and additional subscripts used are

s	= condition at spark
IVC	= condition at inlet valve close
TDC	= condition at top dead center
u	= unburned gas
b	= burned gas

The laminar flame speed was calculated from the expression

$$s_\ell = s_o(\phi)(1 - 2.5f_r)(T/298)^{\alpha}p^{\beta} \qquad (2.1)$$

TABLE 1a

ENGINE GEOMETRY

Bore (Square) (mm)	D	= 82.6
Stroke (mm)	S	= 114.3
Con. Rod Length (mm)	L_c	= 780
Compression Ratio	C_R	= 5.75
Displacement Volume (cm^3)	V_D	= 780
Crevice Volume (cm^3)	V_{cr}	~ 10
IV Diameter (mm)	D_{IV}	= 31.5
IV Lift (mm)	L_{IV}	= 5.7
EV Diameter (mm)	D_{EV}	= 31.5
EV Lift (mm)	L_{IV}	= 6.0
Piston Area/IV Area	A_p/A_{IV}	= 12.1

Timing	θ(°ATC)	$V(\theta)(cm^3)$
IVO	-350	171
EVC	-345	180
IVC	-146	892
TDC	0	164
EVO	140	871
BDC	180	944

TABLE 1b

FIXED OPERATING PARAMETERS

Wall Temperature	T_W = 67 C = 340 K
Speed	N = 1400 RPM
Angular Speed	ω = 8.40 CA°/ms
Mean Piston Speed	u_p = 5.32 m/s
Fuel: Propane	LHV = 46.3 kJ/g
Air Flow Rate	$\dot{m}_A$ = 4.24 g/s
Fuel Flow Rate	$\dot{m}_F$ = 0.237 g/s
F/A Equivalence Ratio	ϕ = 0.87
Residual Mass Fraction	f_r = 0.15 ± .01
IVC Pressure	p_{IVC} = 0.49 atm
IVC Density	ρ_{IVC} = 0.49 g/ℓ
IVC Temperature	T_{IVC} = 355 K

using the values for propane

$$s_o(0.87) = 0.28 \text{ m/s}$$

$$\alpha = 2.22$$

$$\beta = -0.21$$

obtained from Ref 8. The mean inlet speed was calculated from the equation

$$u_{in} = 4(\dot{m}_A+\dot{m}_F)/(\pi\rho_{IVC}D_{IV}L_{IV}) \ . \qquad (2.2)$$

The axial and squish velocities were calculated from simple displacement models and the swirl velocity was calculated using a swirl number of unity obtained from experiments in a plexiglass model.

Cylinder pressures were measured using an RTV coated Kistler pressure transducer and recorded at 1° crank angle intervals using a 12 bit A/D convertor. Prior to spark the pressure curves showed no observable cycle-by-cycle variations and were reproducible within the accuracy of the A/D converter. High speed Schlieren photographs of the flame front were obtained using a Hycam camera run at framing rates $\dot{n}_c$ between 2000 and 2300 frames per second.

The pressure and photographic record were synchronized to the nearest half frame by observing the piston motion on the photographs. The resulting uncertainty of plus or minus one quarter frame produces a "top hat" error distribution of half-width 1.0° in crank angle or 120 μs in time. As will be discussed later, this was a major source of error in the determination of the flame thickness.

Typical photographs and pressure records are shown in Fig. 3. The crank angles at which the photographs were taken are indicated by the letters. Also shown is the burned mass fraction obtained from the pressure record using the thermodynamic model described in Ref 9. Note that although photographs (a) and (b) clearly show substantial burned volume fractions, the corresponding burned mass fractions were too small to be measured. This demonstrates the superiority of photographic

TABLE 2

TEST CONDITIONS AT SPARK

Case:	Base	Squish 1	Squish 2	Shroud
θ_s(°ATC)	-45	-45	-35	-25
V_s(cm^3)	297	297	246	206
V_{IVC}/V_s	3.00	3.00	3.62	4.33
V_s/V_{TDC}	1.87	1.81	1.50	1.26
ρ_s(g/ℓ)	1.47	1.47	1.77	2.12
p_s (atm)	2.09	2.09	2.67	3.38
T_s (K)	505	505	536	567
$(\rho_u/\rho_b)_s$	4.3	4.3	4.2	4.1
$s_{\ell s}$(0) (m/s)	0.76	0.76	0.82	0.89
$s_{\ell s}$(0.15) (m/s)	0.48	0.48	0.51	0.56
u_{ins} (m/s)	60	60	60	120
Ma_{ins}	0.15	0.15	0.15	0.30
u_{AXs} (m/s)	1.8	1.8	0.9	1.6
u_{SQs} (m/s)	-	5.3	7.6	-
u_{SWs} (m/s)	-	-	-	7.5

SQUARE PISTON CHAMBER GEOMETRY

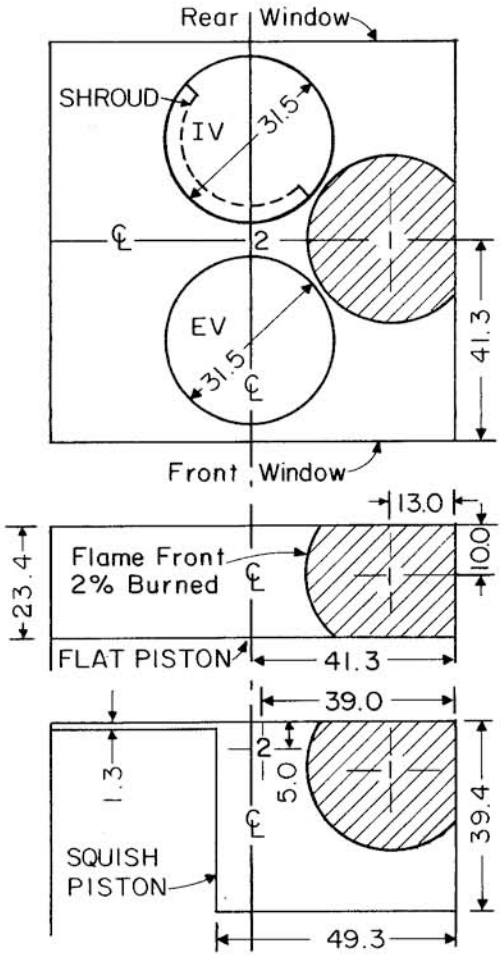

Dimensions in mm; 1 and 2 are spark loci

Fig. 2. Schematic of combustion chamber geometries and spark locations used in experiments. Cases studied were: 1) Base: flat piston, no shroud, spark at 1; 2) Shroud: flat piston, 180 shroud shown by dashed line, spark at 1; 3) Squish: stepped piston, no shroud, spark at 1; 4) Squish: stepped piston, no shroud, spark at 2.

records over pressure measurements for investigating ignition and early flame development.

ANALYSIS OF RESULTS

For each of the four chamber geometries studied, five consecutive cycles were analyzed using the methods of Ref 4 to obtain flame front radii, flame center positions and burned gas radii as functions of time.

GEOMETRICAL PARAMETERS - To obtain the flame front radius and the flame center position, the Schlieren photographs were enlarged, traced by hand and converted to digital form using a tablet digitizer. A

circle having the same area, A_f, and center-of-area as the Schlieren shadow was then fit to the points. The end result was a set of "shadow radii,"

$$r_f \equiv (A_f/\pi)^{1/2}, \tag{3.1}$$

and center coordinates, x_c and y_c, in the plane of the photographs. Due to the difficulty of determining the center-of-area after flame contact with a wall, x_c and y_c were only calculated prior to contact. After contact x_c and y_c were held fixed. The position of the flame center in the z-direction perpendicular to the plane of the photographs was, of course, not observable.

It should be emphasized that Eq. 3.1 constitutes the definition of the shadow radius, r_f, and no assumptions regarding the degree of wrinkling or 3-dimensional properties of the flame front have yet been made.

Two typical flame shadow tracings and corresponding best fit circles for crank angles of 7 and 10 degrees after spark in the same cycle are shown in Fig. 4. Also shown are the burned mass fractions estimated from the relation

$$x_b = \frac{m_b}{m} = \frac{(\rho_b/\rho_u)V_b/V}{1 - (1-\rho_b/\rho_u)V_b/V} \tag{3.2}$$

using the approximation

$$V_b \approx \frac{4}{3}\pi r_f^3 \tag{3.3}$$

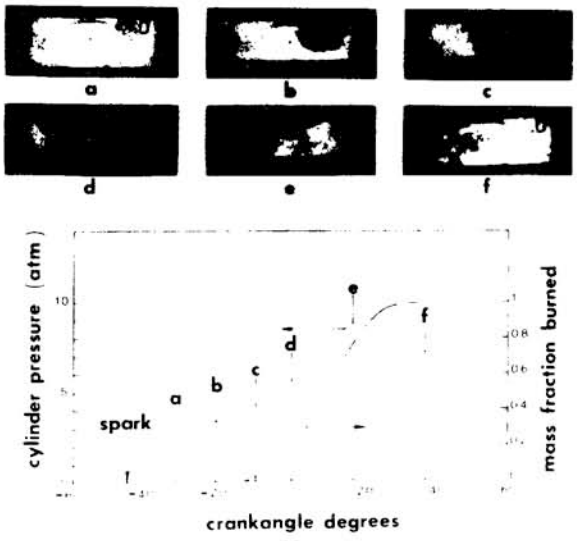

Fig. 3. Example of synchronized Schlieren photographs and pressure record for the Base case. Framing rate was ~ 2000 s^{-1}; synchronization was accurate to ± 100 μs.

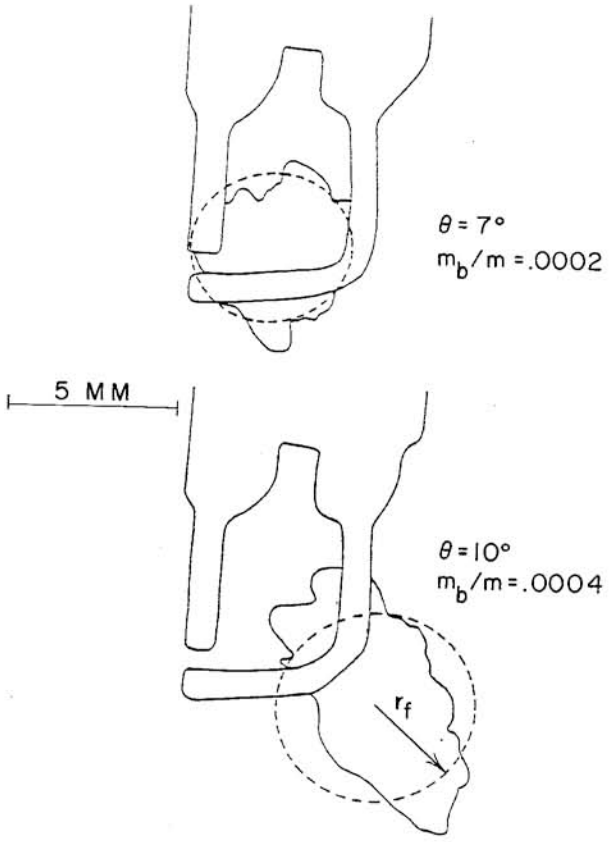

Fig. 4. Tracings showing convection and distortion of early flame kernel "shadow." Dashed circle has same area and center as "shadow."

which is valid for simply-connected roughly-spherical flame fronts. Under conditions where the flame front is highly distorted as in the 10° case in Fig. 4, the error involved in using Eq. 3.3 to calculate burned gas volume V_b is of the same magnitude as the uncertainty in the effective radius of the flame kernel in the z-direction perpendicular to the plane of the shadow. Assuming the distortion in the x-z or y-z planes is similar to that observable in the x-y plane, the estimated error in x_b for the 10° case in Fig. 4 is ± 30%. To the extent that the distortion in successive frames is statistically independent, it can be reduced by smoothing over several frames and this was done. Clearly, however, it would be very valuable to have orthogonal shadows of the flame fronts and a technique for obtaining these is currently being implemented.

It can be seen in Fig. 4 that even at very early times the flame front is quite wrinkled and there is a substantial displacement of the flame center from the spark gap. Clearly the burned mass fractions shown are far too small to be obtained from pressure measurements.

FLAME CENTER MOTION - Plots of the flame center trajectories for all cycles investigated are shown in Fig. 5. The points show

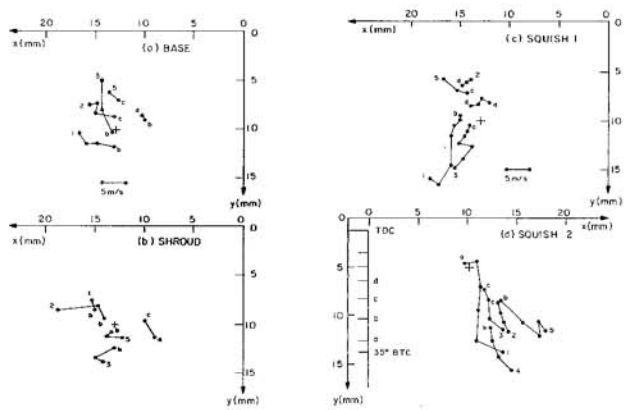

Fig. 5. Trajectories for center of shadow area. Points correspond to frames. Numbers at end of trajectories refer to cycles. See text for further discussion.

the flame center position for each frame for which it could be measured. The letters at the beginning of the trajectories index the frame after spark for which the center position could first be determined i.e. a = first frame, b = second, etc.. The numbers at the end of the trajectories refer to individual cycles. The last point, called the "contact" flame center corresponds to the frame just prior to contact of the flame front with a wall. The horizontal bar terminated by dots shows the distance traveled between frames for a speed of 5 m/s. Table 3 gives the mean values and standard deviations of the contact flame centers.

The character of the trajectories strongly suggests both convection of the flame center by the base flow and "random walk" in the turbulent flow. This is particularly evident in the Squish 2 case where the flame center is convected toward the center of the combustion chamber by the strong squish velocity. A similar convection in the z-direction due to the swirl velocity would also be expected for the Shroud case but this was not observable. There is some indication in the Base case of convection toward the head due to the axial flow and all cases show a slight tendency of the flame center to move away from the side wall. As will be seen later, this early displacement of the flame center from the spark gap is a major cause of cycle-by-cycle fluctuations in the mass burning rates observed later in the cycles.

Table 3

FLAME CENTER DISPLACEMENTS

Mean displacements (mm) of the contact flame centers from the spark location and standard deviation of points about the mean

Case	$\bar{x}_{cs} \pm \delta x_c$	$\bar{y}_{cs} \pm \delta y_c$
Base	0.8 ± 2.1	-2.5 ± 2.1
Shroud	2.8 ± 2.0	0.5 ± 2.4
Squish 1	2.8 ± 1.7	0.2 ± 4.9
Squish 2	4.9 ± 1.7	7.8 ± 1.8

Note: Positive values indicate displacements in a direction away from the walls.

SHADOW RADIUS - Typical plots of r_f and $\dot{r}_f$ as functions of time are shown for the Base case in Figs 6a and 6c. The initial value of r_f was determined from the relation

$$\dot{r}_f\left(\frac{\theta_1 + \theta_s}{2}\right) = \left(\frac{\omega}{\theta_1 - \theta_s}\right) r_{f1} \qquad (3.4)$$

where ω is the angular speed of the engine and the subscript 1 refers to the first frame after spark for which r_f could be measured. This value of r_f is subject to an error of ±1° in θ_s due to the synchronization error previously discussed. Since $\theta_1 - \theta_s$ is on the average ~7°, the resulting error in r_f is about ±15%. By comparison the error in $\dot{r}_f$ due to the estimated error of ±5% in the determination of r_f from Eq 3.1 is negligible.

Subsequent values of $\dot{r}_f$ were determined from the relation

$$\dot{r}_f(\theta_i) = (r_{f,i+1} - r_{f,i-1})\, \dot{n}_c /2 \qquad (3.5)$$

where $\dot{n}_c$ is the framing rate of the camera and the subscripts denote frame number. In this case the error in $\dot{r}_f$ is due entirely to the error in determining the relatively small difference $(r_{i+1} - r_{i-1})$. Representative errors are shown on the plots.

BURNED GAS MASS AND RADIUS - For $(p - p_s) < p_s$, the burned mass fraction can be most accurately determined from the relation (4)

$$x_b = ((p/p_m)^{1/\gamma} - 1)/(\rho_u/\rho_b - 1) \qquad (3.6)$$

where p_m is the polytropic extrapolation of the pressure curve observed prior to spark and γ is the polytropic exponent. For $(p - p_s) > p_s$, the mass fraction burned was obtained from the thermodynamic analysis given in Ref 9.

The burned gas volume was obtained from the relation

$$V_b = m_b/\rho_b = x_b m/\rho_b \qquad (3.7)$$

and corresponding burned gas radius r_b was obtained numerically using definition

$$V(r_b, \underline{r}_c, \theta) = V_b \qquad (3.8)$$

where r_b is the radius of the spherical surface centered at $\underline{r}_c$ containing all and only burned gas and the crank angle θ determines the piston position.

Typical plots of r_b and $\dot{r}_b$ as functions of time are shown in Figs 6b and 6d for the base case. The values of $\dot{r}_b$ were obtained from the relations

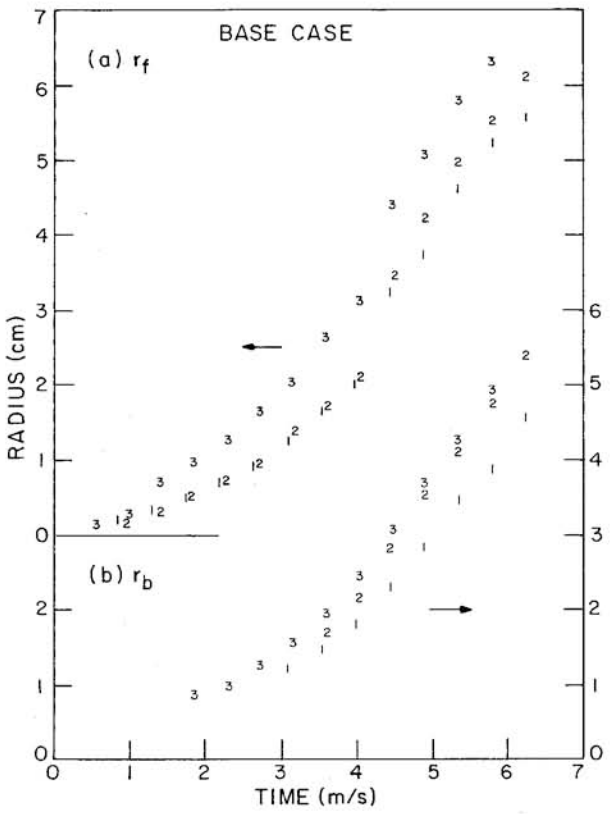

Fig. 6. Typical plots of radii and expansion speeds for burned gases and shadows as a function of time for Base case. Horizontal error bar shows cycle-by-cycle error due to uncertainty in synchronization of photographic and pressure records.

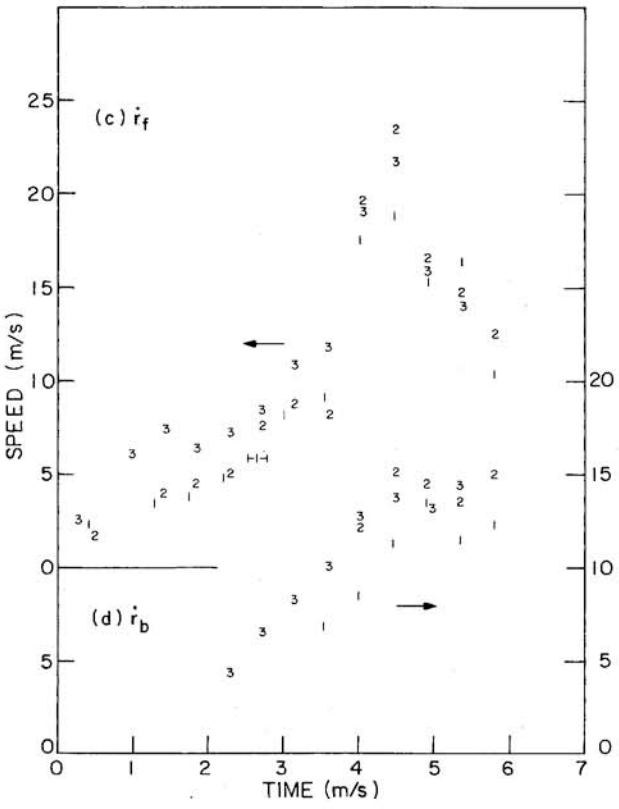

$$\dot{r}_b(\theta_i) = (r_{b,i+1} - r_{b,i+1})\,\dot{n}_c/2 \quad (3.9)$$

Given r_b and $\underline{r}_c$ the spherical burning area $A_b = A(r_b, \underline{r}_c, \theta)$ can be determined from the geometry of a sphere within the combustion chamber. Representative plots of $A(r, \underline{r}_c, \theta)$ as a function of r for $\theta = 0$ and various flame center positions are shown in Fig. 7 for the two pistons used. It can be seen that $A(r, \underline{r}_c, \theta)$ is a strong function of both the radius r and the center coordinates x, y and z. Note especially in Fig. 7b the strong influence of displacement of the flame center in z-direction perpendicular to the photographs. Also note that the derivative dA/dr is discontinuous at points where the spherical front touches a wall.

The burning speed can be determined from the definition

$$s_b = \dot{m}_b/\rho_u A_b \quad (3.10)$$

In this connection it should be noted that since $\dot{m}_b = dm_b/dt$ was determined from smoothed curves of m_b vs. time, discontinuities in ds_b/dr_b occur at points where where dA/dr is discontinuous. Such discontinuities are an artifact associated with the method of data analysis and do not reflect the actual behavior of s_b. In most cases the effect is small and produces only slight irregularities in plots of s_b vs. r_b. An exception is contact with the side walls when the effect is quite large due to the rapid decrease in flame area.

CORRELATION OF PHOTOGRAPHIC AND PRESSURE DATA - Plots of the shadow radius r_f obtained from the Schlieren photographs as a function of the burned gas radius r_b obtained from the pressure measurements are shown in Fig. 8 for all cases studied. The numbers refer to cycles and the four cases have been separated by displacing the origins on the ordinate. It can be seen that r_f approaches r_b for values of r_b less than ~1 cm. For larger values of r_b the value of r_f increases relative to r_b indicating substantial entrainment of unburned gas behind the shadow front. This behavior has been observed in prior experiments (4). There is some indication that the values of $(r_f - r_b)$ approach a steady state but the evidence is weak due to the large scatter of the points. A large part of the cycle-by-cycle scatter may be attributed to the synchronization error between photographic and pressure records. The magnitude of this error may be estimated from the relation

$$\delta r_b \sim \dot{r}_b/4\dot{n}_c \quad (3.11)$$

and is shown by the representative horizontal error bars. In addition frame-by-frame scatter would be expected due to the uncertainty in the effective radius of the flame front perpendicular to the plane of the Schlieren photographs. Close inspection of

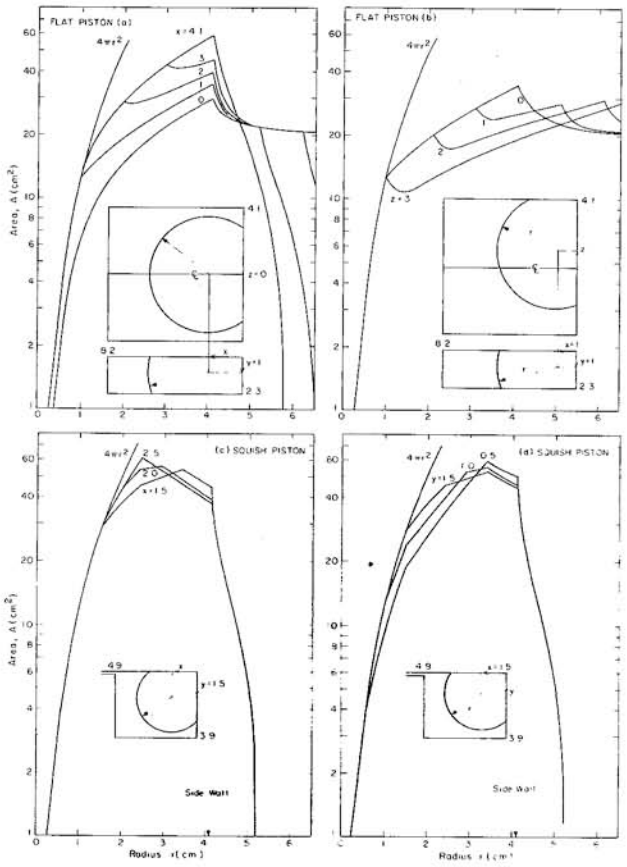

Fig. 7. Typical plots of the spherical burning area as a function of radius showing the effect of center location for both flat and squish pistons.

the data in Fig. 8 suggests that the frame-by-frame scatter is somewhat less than the cycle-by-cycle scatter.

The data in Fig. 8 indicate that for small r_b, the shadow expansion speed $\dot{r}_f$ approaches the burned gas expansion speed $\dot{r}_b$. It follows that the burning speed at early times can be calculated from values of $\dot{r}_f$ using the approximate relation

$$s_b \approx (\rho_b V/m)\ \dot{r}_b \approx (\rho_b V/m)\ \dot{r}_f \equiv s_f \quad (3.12)$$

given in Ref 4. Calculated curves of the factor $m/\rho_b V$ are shown in Fig. 9 as a function of r_b for a typical value of $\rho_u/\rho_b = 4$ and a flame centered at the spark location. The experimental values of s_f are plotted in Fig. 10 as a function of r_f. Also shown is an approximate burned mass fraction scale calculated from the curves in Fig. 9 assuming $r_f \approx r_b$. Only data for $r_f < 20$ mm are shown because for larger radii the values of $\dot{r}_f$ are subject to large uncertainties due to strong wall interactions. It can be seen that s_f increases linearly with radius in the range shown and extrapolates to a value quite close to the expected laminar flame speed s_ℓ. To show this more clearly, least squares fits of

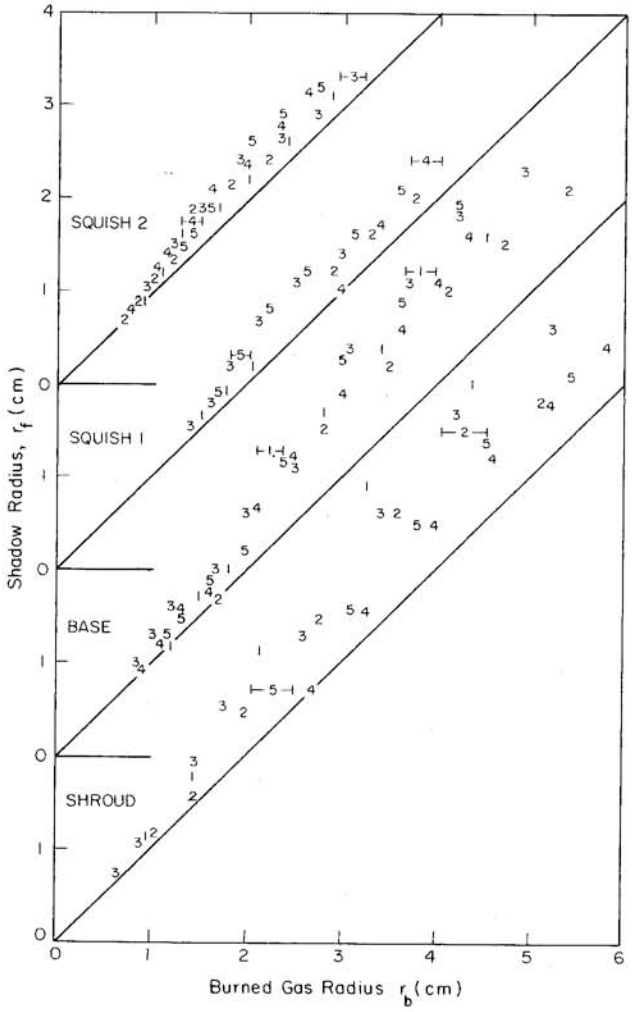

Fig. 8. Correlation of the "shadow" radius r_f and the burned gas radius r_b. Numbers refer to cycles.

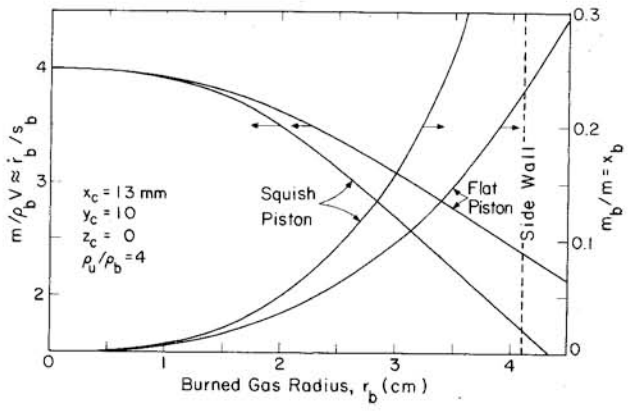

Fig. 9. Calculated curves of the density ratio, $m/\rho_b V$, and mass fraction burned, m_b/m, as a function of burned gas radius for a typical flame front.

all the data for each case were made to the function

$$s_f = s_s + \nu_s r \qquad (3.13)$$

The straight lines represent these fits.

The same procedure was used to fit the data on a cycle-by-cycle basis and the resulting values of the parameters s_s and ν_s are plotted in Fig. 11 as a function cycle number for each case. The error bars represent standard deviations in the fitted parameters due to the scatter of the points. Also shown by the horizontal solid lines are the mean values $\bar{s}_s$ and $\bar{\nu}_s$ for each case. The horizontal dashed lines show the laminar flame speeds calculated from Eq. 2.1 for 0 and 15% residual mass fractions.

It can be seen that the initial burning speeds scatter about the expected values of the laminar burning speed. A possible reason for this could be incomplete mixing of the fresh charge with the residual charge. No variation in equivalence ratio is expected since a mixing tank was employed. There is some indication particularly in the Squish 2 case that the residual fraction at the spark may depend on chamber geometry and spark location. There is little evidence of abnormally high initial speeds due to energy input from the spark. Unfortunately this energy was not monitored but it is estimated to be on the order of millijoules which is roughly equivalent to the chemical energy in one cubic millimeter of mixture.

There is also considerable scatter in the initial slopes. This could be associated with variations in the turbulent intensity at the spark. This would explain the significantly higher values of ν_s observed for the Shroud case. Further discussion of the early flame development is given in the following section.

EDDY BURNING MODEL

The analysis in this section is based on the eddy burning model developed by Keck and co-workers. The original form of these equations proposed by Blizard and Keck (3) was

$$\dot{m}_b = \mu/\tau_b \qquad (4.1)$$

$$\dot{\mu} = \rho_u A_f u_T - \mu/\tau_b \qquad (4.2)$$

where

$$\mu = \rho_u (V_f - V_b) \qquad (4.3)$$

is the unburned mass entrained behind the flame front,

$$\tau_b = \ell_T / s_\ell \qquad (4.4)$$

is a characteristic eddy burning time, u_T is a characteristic turbulent entrainment speed and ℓ_T is a characteristic eddy size. This model was based on the assumption now well supported by experiments (2) that turbulent flames in spark ignition engines can be modeled as thin wrinkled multiply connected laminar flames.

Later in a purely phenomenological analysis by Beretta, Rashidi and Keck (4) of experiments in a glass piston engine by Rashidi (10) it was found that a better fit with the data at early times was obtained by replacing Eq. (4.1) with the modified form

$$\dot{m}_b = \rho_u A_f s_\ell + \mu/\tau_b \qquad (4.5)$$

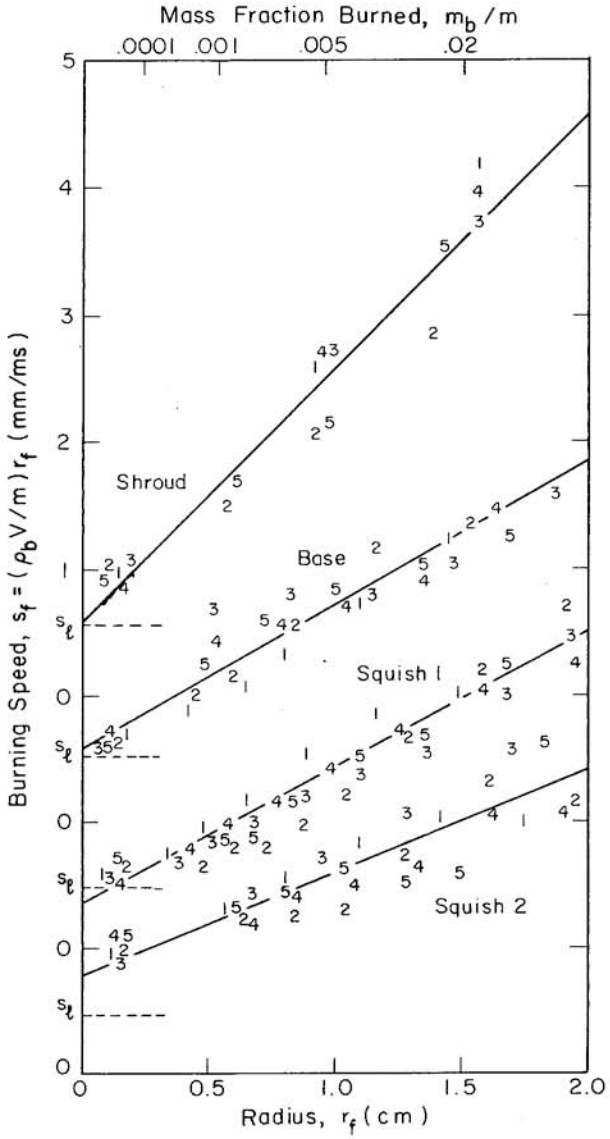

Fig. 10. Plot of burning speed s_f determined from optical data as a function of the radius r_f. Also shown on the top scale is the approximate mass fraction burned m_b/m.

Although the additional term $\rho_u A_f s_\ell$ was deduced empirically, it implies an initial spherical laminar burning phase for the charge. The existence of such a term is completely consistent with the wrinkled laminar flame model and should have been included in the original model on physical grounds.

In the present analysis which includes data at even earlier times than those available in any previous study, a further modification of the equations was required so that they now take the form

$$\dot{m}_b = \rho_u A_b s_\ell + \dot{\mu}/\tau_b \qquad (4.6)$$

$$\dot{\mu} = \rho_u A_b u_T (1 - e^{-t/\tau_1}) - \mu/\tau_b \qquad (4.7)$$

where

$$\tau_1 = \ell_1/s_1 \qquad (4.8)$$

may be interpreted as the burning time of the first eddy burned, ℓ_1 is the size of the first eddy burned, s_1 is the laminar flame speed at the spark and μ and τ_b are given by Eqs 4.3 and 4.4. The introduction of the term $(1 - e^{-t/\tau_1})$ was required to explain the initial flame growth at times less than τ_b. It implies that significant wrinkling of the flame front occurs only after the flame has burned from the site of the spark to the edge of the eddy in which the spark occurred.

Typical curves showing the effect of this term on the calculated burning speeds are shown in Figs 12a and 12b for flat and squish pistons and several values of the ratio ℓ_1/ℓ_T. It can be seen that the initial dependence of s_b on r_b is quite sensitive to the value of ℓ_1/ℓ_T and that the approximately linear dependence of s_b on r_b shown in Fig. 10 is best represented by a value of ℓ_1/ℓ_T = 1. It can also be seen that cycle-by-cycle variations in the size of the first eddy burned produce variations in qualitative agreement with those observable in Fig. 10. In this connection, it should be noted that the effective size of the first eddy burned is expected to depend both on the size of the eddy relative to the length of the spark and the location within the eddy where the spark occurs.

A second relatively minor modification of the equations is the replacement of A_f by A_b. This was required to account for features of the burning curves associated with wall interactions. Both these modifications are justified on physical grounds.

Of the five parameters contained in the model, three u_T, ℓ_T and ℓ_1 are related to the characteristics of the turbulent flow field and two s_ℓ and s_1 to the chemistry of combustion. Although in principle u_T and ℓ_T could be obtained from direct measurements or fundamental turbulence models, no such measurements or models are currently available. These parameters are therefore regarded as unknowns to be obtained by fitting data on burning rates in engines and correlated with engine geometry and operating conditions. Apriori values of s_ℓ based on measurements (8) can be calculated from Eq.(2.1) if the pressure, temperature, equivalence ratio and residual mass fraction of the burning gas are known. However, because of the possibility of incomplete mixing, the residual mass fraction is somewhat uncertain in the vicinity of the spark and therefore s_1 is regarded as an additional unknown to be determined along with u_T, ℓ_T and ℓ_1. In the present analysis s_1 was equated to the values of s_s shown in Fig. 11.

DETERMINATION OF ℓ_T - Combining Eqs 4.3, 4.4 and 4.6 and using the definitions for the burning speed $s_b = \dot{m}/\rho_u A_b$ and laminar burning area $A_\ell = \dot{m}_b/\rho_u s_\ell$, we obtain the equation

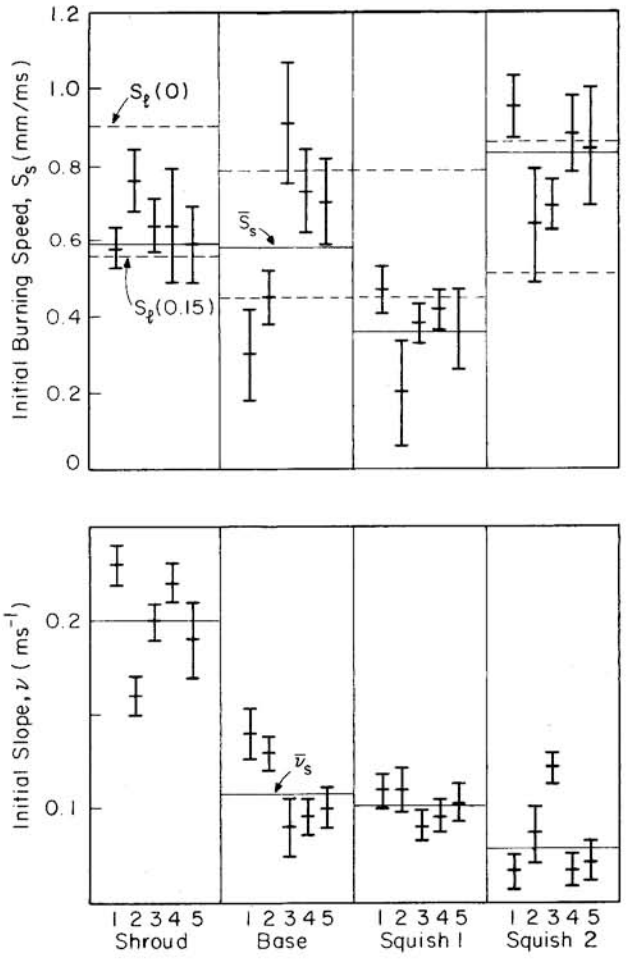

Fig. 11. Parameters obtained by a least squares fit of the equation $s_f = s_s + \nu_s r_f$ to the data in Fig. 10. Also shown are the laminar burning speeds $s_\ell(0)$ and $s_\ell(0.15)$ for 0 and 15% residual mass fraction.

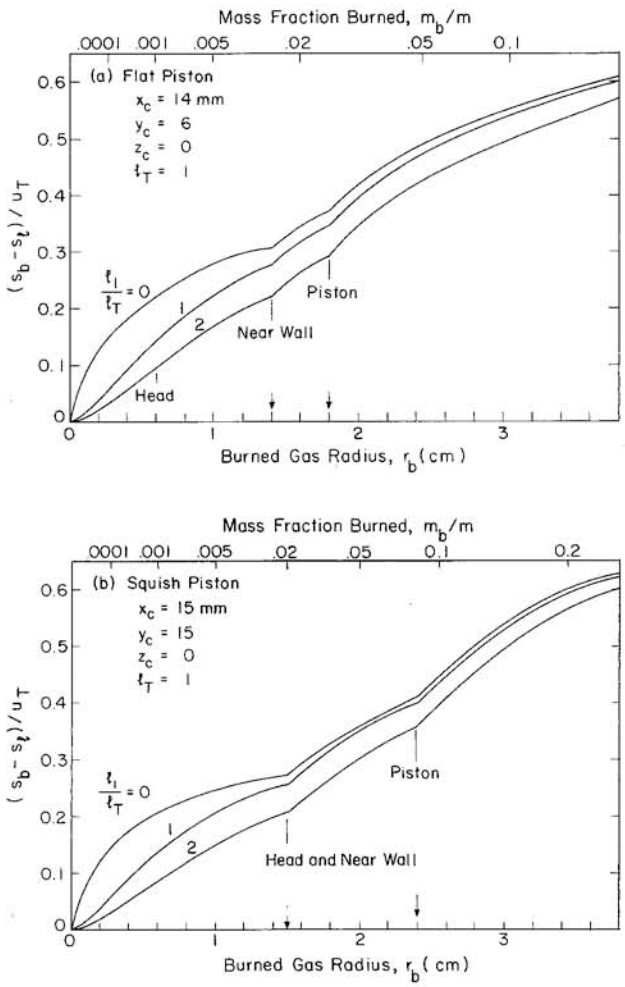

Fig. 12. Calculated curves showing the effect of the ratio ℓ_1/ℓ_T on the speed ratio $(s_b - s_l)/u_T$ for typical flame fronts and flat and squish pistons.

$$\ell_T = (V_f - V_b)/(A_l - A_b) \qquad (4.9)$$

Introducing the approximation

$$V_f \approx V_b + A_b(r_f - r_b) \qquad (4.10)$$

valid for $(r_f - r_b) \ll r_b$, we obtain the more convenient relation

$$\ell_T \approx (r_f - r_b)/(s_b/s_l - 1) \qquad (4.11)$$

which relates ℓ_T directly to the flame thickness. The values of ℓ_T calculated from Eq. 4.11 are plotted in Fig. 13 as a function of r_b.

Because of the extreme sensitivity of the small difference $(r_f - r_b)$ to errors in r_f and r_b only data for which $m_b/m > 0.01$ and wall interactions were negligible are included in Fig. 13. Over the narrow range covered there is no significant dependence of ℓ_T on r_b and the points for each case were averaged to obtain the values shown by the horizontal lines. The error bars were calculated using Eq. (3.11) and show the uncertainty due to synchronization of the photographic and pressure records. Within the errors involved, ℓ_T = 1.0 ± 0.2 mm for all cases. Since the ratio in the clearance heights for the squish and flat pistons was roughly 2, this supports evidence from previous studies (2) that clearance height has relatively little effect on ℓ_T. Comparing the shroud case with the remaining cases we also conclude in agreement with prior work (2) that inlet gas speed has little effect on ℓ_T. This is puzzling theoretically but convenient practically.

DETERMINATION OF u_T AND ℓ_1 - To determine u_T and ℓ_1 a trial and error fitting procedure was used. In accord with previous findings (2) and the predictions of rapid distortion theory (11), u_T and ℓ_T were assumed to have the functional forms

$$u_T = u_{Ts} (\rho_u/\rho_{us})^{1/2} \qquad (4.12)$$

and

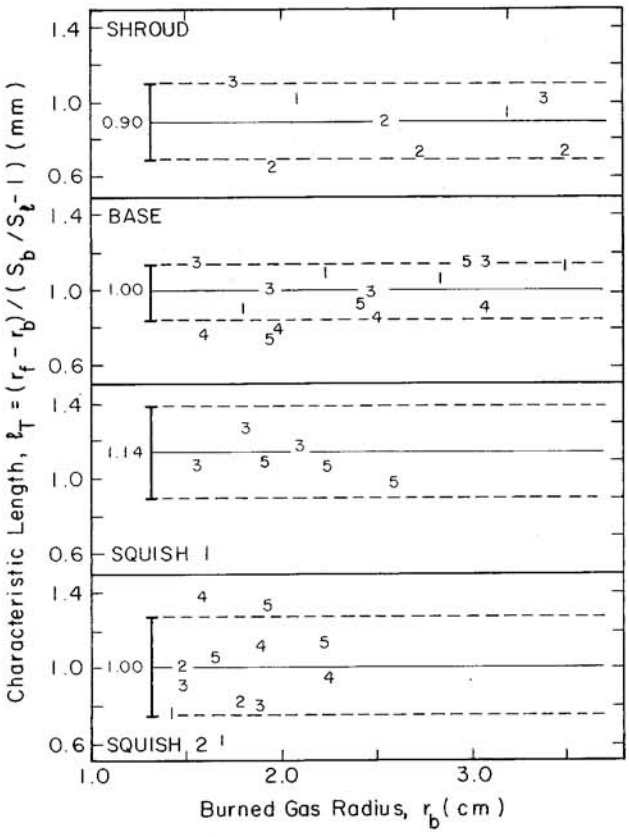

Fig. 13 Plots of the characteristic length $\ell_T = (r_f - r_b)/(s_b/s_l - 1)$ as a function of r_b. Only points for which m_b/m > 1% and wall interactions were negligible are shown. The solid lines are mean values; the dashed lines show the error due to the 100 μs uncertainty in synchronization of optical and pressure records.

$$\ell_T = \ell_{Ts}(\rho_{us}/\rho_u)^{3/4} \qquad (4.13)$$

Using the measured values of $r_b(t)$ and the previously determined values of the parameters s_ℓ, s_1 and ℓ_{Ts}, Eq. (4.7) was integrated numerically for various trial values of u_T^s and ℓ_1 to obtain $\mu(t)$ which was then substituted into Eq. (4.6) to obtain values of $\dot{m}_b/\rho_u = s_b A_b$ for comparison with experimental data. The results of this procedure are shown in Fig. 14 and values of the best fit parameters are summarized in Table 4.

One of the surprising and interesting features of this comparison, is the relatively small cycle-by-cycle fluctuations in the burning rates for the Squish 2 case in Fig. 14d. By way of contrast the cycle-by-cycle fluctuations for the Shroud case in Fig. 14b are relatively large, particularly for values of r_b greater than 2 cm. Examination of the positions of the contact centers, also shown on the figures, indicates that these fluctuations are caused primarily by cycle-by-cycle variations in the positions of the contact flame centers with respect to the walls. In the Squish 2 case the contact flame-centers are all relatively far from the walls so that the variations in the burning area A_b caused by wall interactions are minimal over the range of r_b covered by the data. In addition, the dispersion of the flame centers is relatively small. In the Shroud case the stable flame centers are much closer to the walls and the dispersion is considerably larger. Moreover substantial displacements (not observable) of several centimeters in the z-direction are expected due to the high swirl velocity at the spark. As can be seen in Fig. 7b, this causes substantial variations in the burning area which are directly reflected in the burning rate. The magnitude of the effect is illustrated by the dashed curve in Fig. 14b which was calculated for $z_c = 3$ cm and fits the data for cycle 4 reasonably well. The other cycles may be fit with intermediate values of z_c. It should be noted in this connection that in a circular cylinder, changes in flame area due to swirl-produced flame center motion would be absent, since a swirling flow produces no radial displacement toward or away from the cylinder walls.

The same effects are also apparent in the Base and Squish 1 cases shown in Figs 14a and 14c. In the Base case the dispersion of cycles 1, 2, 3 and 5 is relatively small. Cycle 4 is clearly different but it can be fit by an assumed value of $z_c = 1.5$ cm. This is larger than the observed x_c and y_c dispersions, but is not unreasonable. The Squish 1 data show intermediate dispersions which correlate quite well with the observed positions of the contact flame centers.

TABLE 4

Summary of Model Parameters

a) Eddy Burning Parameters

Case	$s_{\ell s}$	$s_1 \pm \delta s_1$	u_{Ts}	ℓ_{Ts}	$\ell_1 \pm \delta\ell_1$
	m/s	m/s	m/s	mm	mm
Base	0.48	0.58 ± 0.18	8	1.4	1.4 ± 0.3
Squish 1	0.48	0.36 ± 0.13	7	1.4	1.4 ± 0.3
Squish 2	0.51	0.80 ± 0.16	7	1.4	1.4 ± 0.4
Shroud	0.56	0.59 ± 0.19	14	1.4	1.4 ± 0.3

(b) Characteristic Times at Spark (ms)

Case	$\tau_T = \frac{\ell_T}{u_T}$	$\tau_b = \frac{\ell_T}{s_\ell}$	$\tau_c = \frac{\alpha}{s_\ell^2}$	$\tau_D = \frac{\ell_T^2}{\nu}$	τ_E
Base	0.16	2.9	0.13	100	43
Squish 1	0.20	2.9	0.13	100	43
Squish 2	0.20	2.7	0.12	100	43
Shroud	0.10	2.5	0.10	100	43

(c) Dimensionless Ratios

Case	$\frac{\ell_T}{\delta_\ell} = \frac{\nu\tau_D}{\alpha\tau_b}$	$\frac{u_T}{s_\ell} = \frac{\tau_b}{\tau_T}$	$\frac{u_T\ell_T}{\nu} = \frac{\tau_D}{\tau_T}$	$\frac{\tau_c}{\tau_T} = \frac{u_T}{s_\ell}\frac{\delta_\ell}{\ell_T}$	$\frac{\tau_D}{\tau_E} = \frac{\ell_T^2}{\nu\tau_E}$
Base	25	18	630	0.8	2.3
Squish 1	25	16	500	0.7	2.3
Squish 2	26	15	500	0.6	2.3
Shroud	27	25	1000	1.0	2.3

ν = kinematic viscosity = 0.2 cm²/s, α = thermal diffusivity = 0.3 cm²/s

The most important conclusion which can be drawn from the comparisons in Fig. 14 is that variations in the position of the contact flame centers caused by "random walk" of the small flame kernel in the turbulent flow field prior to any measurable rise in pressure were the major cause of cycle-by-cycle fluctuations in the burning rate observed later in the cycles. In this connection it should be noted that although convection in the mean flow can alter the mean burning rate it does not produce cycle-by-cycle variations since the mean flow is the same for each cycle. Within the experimental errors, no significant cycle-by-cycle variations in either u_T or ℓ_T were observed during the main combustion stage indicating that random fluctuations in these quantities were effectively averaged out over the large flame area occurring during this stage.

As can be seen in Fig. 10, and to a lesser extent in Fig. 14, significant cycle-by-cycle fluctuations in the early burning rate were also observed. As previously discussed, the most probable cause of these fluctuations is cycle-by-cycle variations in the initial burning speed s_1 and the size ℓ_1 of the first eddy burned. The values and standard deviations of these parameters obtained from the cycle-by-cycle fit of the data are shown in Table 4a. Fluctuations in ℓ_1 are to be expected due to the statistical nature of turbulence. Fluctuation in s_1 can be caused either by fluctuations in the equivalence ratio or the residual mass fraction. Since a mixing tank was used in the present experiments no fluctuations in the equivalence ratio are expected and the fluctuations in s_1 must be attributed to incomplete in-cylinder mixing of the fresh charge with the residuals.

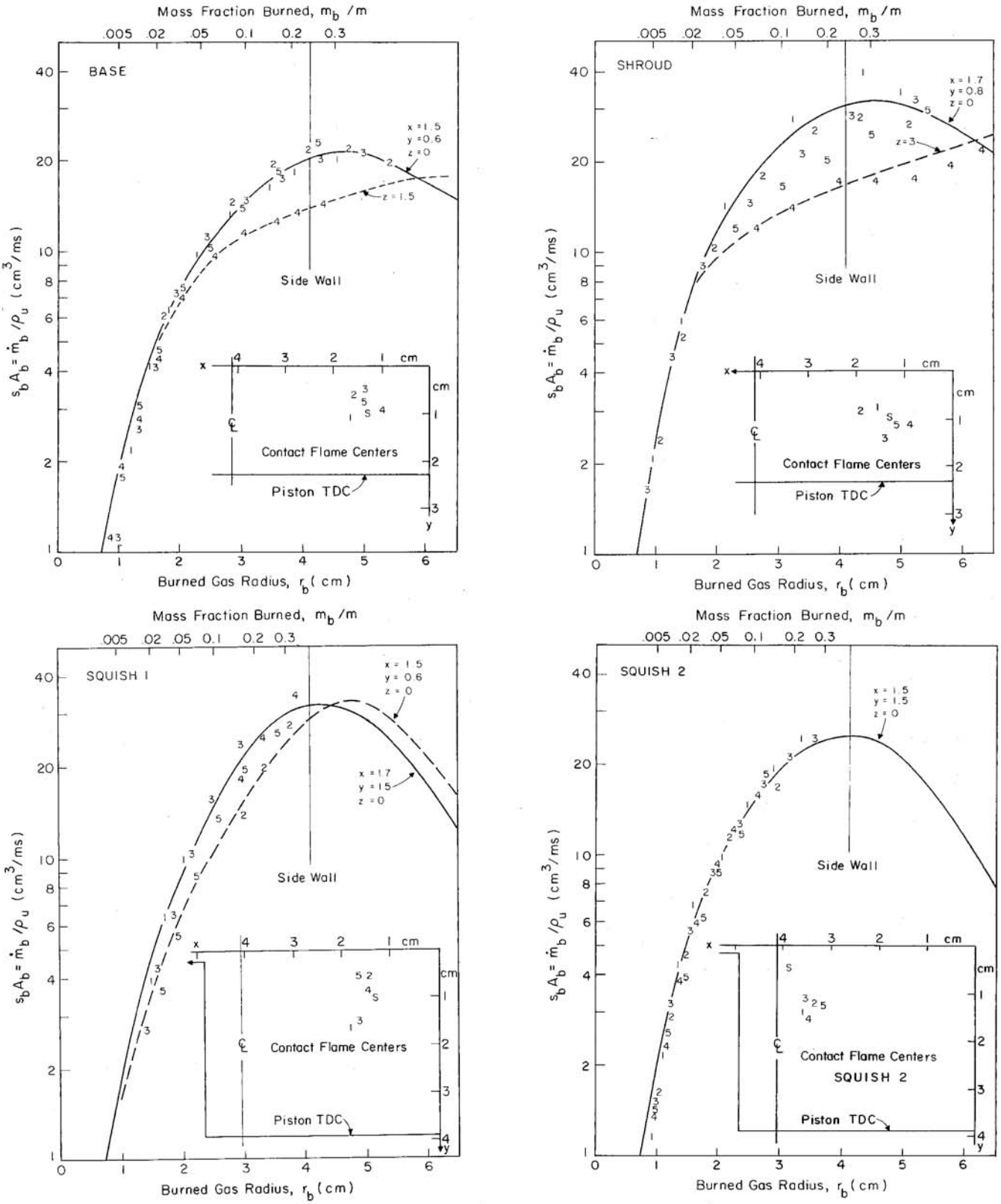

Fig. 14. Plot of volume burning rates $m_b/\rho_u = s_y A_b$ as a function of r_b for the various geometries studied. Also shown are the positions of the "contact" flame-centers for each cycle. The representative curves were calculated from the eddy burning equations using the parameters in Table 4 and the flame center positions indicated.

DISCUSSION AND CONCLUSIONS

A correlation based on previous experiments for predicting the parameters ℓ_{T_s} and u_{T_s} from engine geometry and operating conditions is given in Ref 2. For the Base, Squish 1 and Squish 2 cases, all of which had the same valve lift and inlet speed, the values of ℓ_{T_s} and u_{T_s} obtained from the correlations are 2.0 mm and 8 m/s. For the Shroud case which had the same valve lift but twice the intake speed the values are 2.0 mm and 16 m/s. Considering the errors involved these values are in satisfactory agreement with those in Table 4a. In this connection it should be emphasized again that the largest source of error in the present measurements was the 120 μs uncertainty in the synchronization of the photographic and pressure records. There was also the possibility of an error in the spark timing since this was not directly monitored. In future experiments of this type it is recommended that both these quantities be carefully measured with a precision better than ± 20 μs. The errors associated with assumption of roughly spherical symmetry are expected to be somewhat smaller than those associated with synchronization. As previously discussed, these errors could be reduced by obtaining orthogonal views of the developing flame fronts.

The data in Table 4a can also be used to estimate a number of characteristic times and ratios which may be useful for obtaining better physical insight into the meaning of the present results and the nature of turbulent combustion in premixed spark-ignition engines. These are listed in Tables 4b and 4c. The parameters in Table 4b are: the eddy lifetime, $\tau_T = \ell_T/u_T$; the eddy burning time, $\tau_b = \ell_T/s_\ell$; the characteristic chemical time, $\tau_c = \alpha/s_\ell^2$; the characteristic diffusion time based on eddy size, $\tau_D = \ell_T^2/\nu$; and, the engine cycle time, τ_E. In the above definitions α and ν are the thermal diffusivity and kinematic viscosity. It is not possible to calculate the Kolmogorov time scale because the flow is unsteady and the dissipation rate is unknown. However, if it has any meaning in this context, it is estimated to be less than 1 μs.

It can be seen in Table 4c that the ratio ℓ_T/δ_ℓ is ~25. Thus the assumption of a thin wrinkled laminar flame seems well justified in this case. Also the ratio u_T/s_ℓ is greater than 15 in all cases so that the steady-state turbulent burning-speed is high compared to the laminar flame-speed and the degree of wrinkling and flame stretching is very large. The Reynolds number $u_T\ell_T/\nu$ is of order 10^3 indicating that viscous dissipation is relatively small. The ratio τ_c/τ_T is, however, of order one indicating that shear may play a role in modifying the laminar flame speed. Finally the ratio τ_D/τ_E is ~2 suggesting that laminar diffusion during the intake and compression stroke may be important in determining the characteristic eddy size ℓ_T. In this connection it should be noted that enlarged Schlieren photographs of the flame fronts show no evidence of wrinkling on a scale less than ℓ_T suggesting that smaller scale structure probably does not exist.

The above observations support the conclusion that turbulent flames in premixed spark-ignition engines are thin wrinkled multiply-connected flames propagating locally at or close to the laminar flame speed. What determines the characteristic eddy size is not clear at this time. Neither is the importance of shear in modifying the local laminar flame speed. More work is needed on these problems.

The following additional conclusions may also be drawn from the analysis:

1) Comparisons of "flame shadow" radii measured optically and burned gas radii determined from pressure measurements strongly support a wrinkled laminar flame model of turbulent burning in spark-ignition engines.

2) At early times the expansion speed of the flame kernel increases approximately linearly with burned gas radius and extrapolation to zero radius gives initial speeds which scatter about the estimated laminar flame speed.

3) The most important parameters controlling the initial flame growth are the laminar flame speed at the spark plug s_1 and the size of the first eddy burned ℓ_1. There was no evidence of a significant increase in the initial flame speed due to energy input from the spark although this could be important for higher energy sparks.

4) The most important parameters controlling the fast burning stage of combustion are the spherical burning area A_b and the characteristic turbulent entrainment speed u_T.

5) The transition from the initial to the fast-burning stage is controlled by the characteristic eddy size ℓ_T.

6) There is little evidence of significant cycle-by-cycle variation in u_T or ℓ_T due presumably to averaging of these parameters over the flame front.

7) During early burning, substantial displacement of the flame center from the spark plug occurs due to convection by the mean flow and "random walk" in the turbulent flow.

8) The spherical burning area is a strong function of the position of the flame center at the time the flame first contacts a wall.

9) The major cause of cycle-by-cycle variations in the burning rate during the fast burning stage of combustion is the variation in the spherical burning area produced by variations in the position of the

wall contact flame center.

10) The major causes of cycle-by-cycle variations early in the flame development process are variations in the laminar flame speed at the spark s_1 and fluctuations in the size ℓ_1 of the first eddy burned.

11) The eddy burning model developed by Keck and co-workers can be used to obtain quantitative values of the parameters s_1, ℓ_1, ℓ_T and u_T.

12) For the engine operating condition employed, the values of ℓ_T found were the same for all four chamber geometries studied.

13) Within experimental error, u_T was proportional to mean gas speed through the inlet valve.

14) The values u_T and ℓ_T obtained in the present work are in reasonable agreement with previously published correlations obtained from data on engines without significant swirl or squish.

ACKNOWLEDGEMENT

The authors would like to thank Dr. Jan Gatowski for valuable discussions concerning the details of his experiments. This work was supported by the M.I.T. Sloan Automotive Laboratory's Consortium for Engine Research. Member companies are: Caterpillar Tractor Company, Cummins Engine Company, John Deere Company, Ford Motor Company and GIE Peugeot/ Renault.

REFERENCES

(1) Gatowski, J.A. and Heywood, J.B., "Effects of Valve-Shrouding and Squish on Combustion in a Spark-Ignition Engine," SAE paper 85209, International Fuels and Lubricants Meeting and Exposition, Tulsa, Oklahoma, Oct. 21-24, 1985.

(2) Keck, J.C., "Turbulent Flame Structure and Speed in Spark-Ignition Engines," Proceedings of Nineteenth Symposium (Int'l) on Combustion, The Combustion Institute, pp. 1451-1466, 1982.

(3) Blizard, N.C. and Keck, J.C., "Experimental and Theoretical Investigation of Turbulent Burning Model for Internal Combustion Engines, SAE paper 740191, SAE Automotive Engineering Congress, February 25-March 1, 1974; SAE Transactions, Vol. 83 (1974).

(4) Beretta, G.P., Rashidi, M. and Keck, J.C., "Turbulent Flame Propagation and Combustion in Spark-Ignition Engines," Combustion & Flame, Vol. 56, pp. 71-81, 1984.

(5) Libby, P.A. and Bray, K.N.C., "Implications of the Laminar Flamelet Model in Premixed Turbulent Combustion," Combustion," Comb. Flame 39 33, (1980).

(6) Namazian, M. Hansen, S.P., Lyford-Pike, E.J., Sanchez-Barsse, J., Heywood, J.B., and Rife, J., "Schlieren Visualization of the Flow and Density Fields in the Cylinder of a Spark-Ignition Engine," SAE paper 800044, SAE Transactions, Vol. 89 (1980).

(7) Gatowski, J.A., Heywood, J.B. and Deleplace, C., "Flame Photographs in a Spark-Ignition Engine," Combustion & Flame, Vol. 56, pp. 71-81.

(8) Metghalchi, M. and Keck, J.C. "Burning Velocities of Mixtures of Air with Methanol, Isooctane, and Indolene at High Pressure and Temperature," Combustion and Flame, Vol. 48, pp. 191-210, 1982.

(9) Gatowski, J.A., Balles, E.N., Chun, K.M., Nelson, F.E., Ekchian, J.A. and Heywood, J.B., "Heat Release Analysis of Engine Pressure Data," 1984.

(10) Rashidi,M., The Nature of Cycle-by-Cycle Variations in the S.I. Engine from High Speed Photographs," Comb. & Flame, 42, p.111,(1981.)

(11) Wong, V.W. and Hoult, D.P., "Rapid Distortion Theory Applied to Turbulent Combustion," SAE paper 790357, SAE Transactions, Vol. 88, (1979).